Conformation and Membrane Position of the Region Linking the Two C2 Domains in Synaptotagmin 1 by Site-Directed Spin Labeling[†]

Hao Huang and David S. Cafiso*

Department of Chemistry and Biophysics Program, University of Virginia, Charlottesville, Virginia 22904-4319

Received August 5, 2008; Revised Manuscript Received September 19, 2008

ABSTRACT: Synaptotagmin 1 (syt1) is an integral membrane protein localized on the synaptic vesicle that acts as the Ca^{2+} sensor for neuronal exocytosis. Synaptotagmin 1 contains two C2 domains, C2A and C2B, which bind Ca^{2+} ions, membranes, and SNAREs. Here, site-directed spin labeling (SDSL) was used to determine the position and dynamics of the region that links the two C2 domains in a water soluble construct encompassing the two C2 domains (syt1C2AB). An analysis of the EPR line shapes from this region indicates that the linker is flexible and unstructured when syt1 is in solution or bound to lipid bilayers. The nanosecond dynamics of the linker does not change, in the presence or absence of Ca^{2+}, suggesting that there is no Ca^{2+}-dependent intramolecular association between the two domains. When syt1C2AB is membrane-bound, the position of the linker relative to the membrane interface was determined by measuring parameters for the collision of the spin-labeled syt1C2AB mutants with both soluble and membrane-bound Ni(II) chelates. These data indicate that the linker does not penetrate the membrane surface but lies approximately 7−10 Å from the bilayer surface. In addition, the linker remains flexible when syt1C2AB binds to the SNARE complex, indicating that direct interactions between this linker and the SNAREs do not mediate association. These data suggest that the two C2 domains of syt1 interact independently on the membrane interface, or when bound to SNAREs.

Neurotransmitter release is the result of a highly regulated Ca^{2+}-triggered fusion event that is coordinated by a large number of proteins within the presynaptic cell (*1*−*3*). Soluble *N*-ethylmaleimide-sensitive factor attachment receptor (SNARE)[1] proteins are membrane and membrane-associated proteins that assemble into a highly stable helical bundle that bridges the synaptic vesicle and the plasma membrane within the presynaptic cell. These SNARE proteins are essential for the fusion process, but they do not appear to act as the Ca^{2+} sensor in neuronal exocytosis. The available evidence suggests that synaptotagmin 1 (syt1), a protein composed of two C2 domains, acts as the Ca^{2+} sensor in neuronal exocytosis (*4*−*6*); however, the mechanism by which syt1 acts to trigger SNARE-mediated fusion is not understood. For example, syt1 might directly bind to and regulate the SNAREs (*7*); syt1 might bind membranes and create curvature strain within the bilayer at the site of fusion (*8*), or syt1 might bridge the vesicle and the plasma membrane, driving these two membranes closer together (*9, 10*).

Synaptotagmin 1 is anchored to the synaptic vesicle through a single transmembrane segment located near its N-terminus, where the two water soluble C2 domains, C2A and C2B, are positioned on the C-terminal side of the transmembrane anchor. The two C2 domains are connected by a short linker region and are known to bind to membranes containing negatively charged lipid in a Ca^{2+}-dependent fashion (*5, 6*). When present as a water soluble fragment of syt1 containing both C2A and C2B (syt1C2AB) (see Figure 1), the two domains penetrate the bilayer surface in a Ca^{2+}-dependent fashion so that the first and third Ca^{2+}-binding loops of each domain are inserted into the bilayer (*11*). This fragment is also found to associate with the SNARE complex, and there are reports that both C2A and C2B are responsible for the interactions with SNAREs. For example, NMR studies indicate that there are multiple binding sites for the syt1C2AB−SNARE interaction (*12*), and single-molecule FRET studies imply that the C2B domain or the linker region of syt1C2AB may associate with SNAREs (*13*).

High-resolution structural models for the individual C2A and C2B domains have been obtained (*14*−*17*), and recently, a Ca^{2+}-free structure of syt1 C2AB was determined (*18*). In this crystal structure, the two C2 domains interact, so that the Ca^{2+}-binding loops of C2A interact near the helix on C2B that connects strands 7 and 8. Several residues within the linker region, such as E267 and E271, also appear to make tertiary contact in this structure. Evidence of a direct interaction between the two C2 domains in syt1C2AB has

[†] This work was supported by National Institutes of Health Grants GM 62305 and GM 072694.

* To whom correspondence should be addressed: Department of Chemistry, McCormick Road, University of Virginia, Charlottesville, VA 22904-4319. E-mail: cafiso@virginia.edu. Telephone: (434) 924-3067. Fax: (434) 924-3567.

[1] Abbreviations: DOGS-NTA-Ni(II), 1,2-dioleoyl-*sn*-glycero-3-{[*N*-(5-amino-1-carboxypentyl)iminodiacetic acid]succinyl} (nickel salt); EPR, electron paramagnetic resonance spectroscopy; LUV, large unilamellar vesicle; MTSL, (1-oxy-2,2,5,6-tetramethylpyrroline-3-methyl) methanethiosulfonate; $PI(4,5)P_2$, phosphatidylinositol 4,5-bisphosphate; POPC, palmitoyloleoylphosphatidylcholine; POPS, palmitoyloleoylphosphatidylserine; R1, spin-labeled side chain produced by derivatization of a cysteine with MTSL; SDSL, site-directed spin labeling; SNARE, soluble *N*-ethylmaleimide-sensitive factor attachment receptor; syt1, synaptotagmin 1; syt1C2AB, soluble fragment of synaptotagmin 1 containing the C2A and C2B domains; syn1C2A, C2A domain of synaptotagmin 1.

10.1021/bi801470m CCC: $40.75
Published on Web 10/29/2008

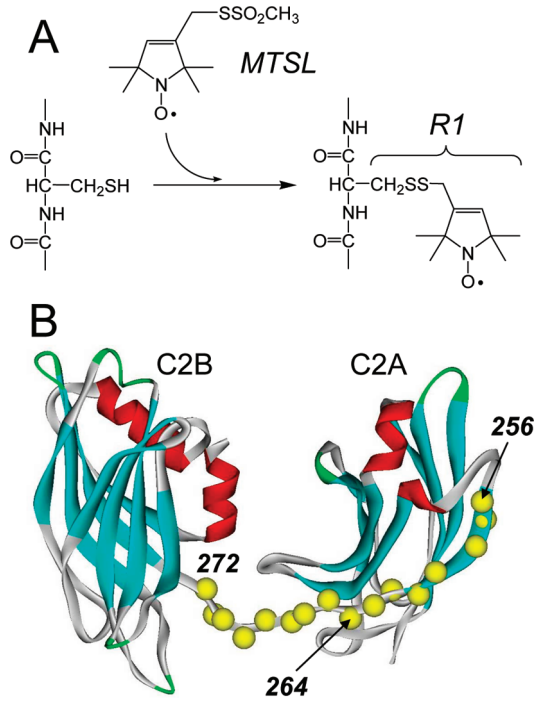

FIGURE 1: (A) Spin-labeled side chain R1 incorporated into syt1C2AB by derivatizing cysteine mutants with the MTSL. (B) Model of a soluble portion of synaptotagmin 1 encompassing the two C2 domains. The first domain, C2A, includes residues 140−263; the second, C2B, includes residues 273−418. The segment linking the two domains is formed from residues 264−272. Here, 16 single-cysteine mutants of a soluble fragment of syt1 (96−421) were produced (Cα positions colored yellow). The C2AB model shown was built from models for the isolated C2A [Protein Data Bank (PDB) entry 1BYN] and C2B (PDB entry 1K5W) domains, which were connected with a linker using InsightII.

also been obtained by FRET, but in this case, Ca^{2+} appears to induce an association of the two domains (*19*). In contrast to these two studies, NMR spectra of the soluble syt1C2AB fragment indicate that the two domains do not interact with each other in solution (*9*); however, there may be conditions, bound to membranes or bound to SNAREs, under which the two domains associate.

Site-directed spin labeling (SDSL) is an EPR-based method that is particularly sensitive to the local structure and dynamics at the labeled site, and SDSL can be utilized to examine proteins in solution, proteins that are bound membranes, or proteins that are part of large complexes (*20*−*24*). In this work, we use SDSL to examine the state of the region that links C2A and C2B in the soluble fragment of synaptotagmin 1 (syt1C2AB). Sixteen single-cysteine mutants of syt1C2AB were expressed and derivatized with a sulfhydryl reactive spin-label (Figure 1A) to incorporate the spin-labeled side chain R1 into sites covering the eighth β-strand of C2A and the linker region that connects the two C2 domains in syt1C2AB (see Figure 1B). In solution, the EPR data indicate that the linker is dynamic and unstructured, in the presence or absence of Ca^{2+}. Furthermore, the linker remains disordered when syt1C2AB is bound to lipid bilayers composed of POPC and POPS. When the sample is membrane-bound, the collision accessibility to a surface-associated Ni(II) complex indicates that the linker does not penetrate the bilayer but lies approximately 7−10 Å from a plane defined by the lipid phosphates. The flexibility of the linker is maintained when syt1C2AB binds to the soluble SNARE complex, indicating that the linker does not directly participate in the interactions with the SNAREs. Taken together, these data indicate that the two C2 domains do not associate but remain structurally independent under a wide range of conditions.

MATERIALS AND METHODS

Mutagenesis, Protein Expression, and Purification. DNA encoding residues for the C2A domain (96−265) and the C2A and C2B domains (96−421) of rat synaptotagmin 1 (P21707) in vector pGEX-KG were obtained from C. Creutz (Pharmacology Department, University of Virginia). The single native cysteine residue at position 277 of syt1C2AB was mutated to alanine by typical polymerase chain reaction (PCR) strategies. All DNA modifications followed published protocols (*25*). Single-cysteine mutants of syt1C2A or syt1C2AB were prepared using either a two-step PCR or a QuickChange site-directed mutagenesis kit (Stratagene, La Jolla, CA), and individual cysteine residues were introduced at positions 170, 176, 189, 193, 202, 217, 239, 240, and 256 of the syt1C2A domain and into positions 256−258 and 260−272 of syt1C2AB (Figure 1) All cysteine substitutions were confirmed by DNA sequencing.

The expression and purification syt1C2AB were carried out as described previously (*11*). Briefly, the construct was encoded in frame with glutathione *S*-transferase (GST), and mutant plasmids for GST-syt1C2AB were transformed into BL21(DE3)pLysS cells (Promega, Madison, WI) and grown. Following affinity purification, steps were taken to remove residual GST and thrombin, and an additional anion exchange step was added to remove nucleic acid contaminants associated with the protein as described previously (*26*). This fragment of syt1 consists of residues 96−421 from syt1 and 13 additional residues from the pGEX vector on the N-terminus. Protein purity and identity were confirmed by SDS−PAGE, and the purified protein was found to bind to Tb^{3+}, using an assay described previously (*11*). Isolated syt1C2AB bound to POPC/POPS vesicles in a Ca^{2+}-dependent manner as judged using a sucrose-loaded vesicle sedimentation assay (*27*) and appeared to be correctly folded as indicated by CD spectroscopy and FTIR.

The synaptotagmin 1 C2A domain was also expressed as a GST fusion protein and was purified using GST affinity chromatography as described in a previous protocol (*28*). Purification of syt1C2A did not require the anion exchange step that was necessary for the purification of syt1C2AB.

The DNA of His_6-tagged soluble SNARE motif fusion proteins, syntaxin 1A, SNAP-25, and synaptobrevin encoded in vector pET-28a were kindly provided by R. Jahn and D. Fasshauer (Max-Plank-Institute for Biophysical Chemistry, Göttingen, Germany). The sequences covered were syntaxin residues 180−262, SNAP-25 residues 1−206, and synaptobrevin residues 1−96. All recombinant proteins were expressed as His_6-tagged fusion proteins and purified by Ni^{2+}-Sepharose affinity chromatography as described previously (*29*). All proteins were further purified by ion exchange chromatography using HiTrap Q HP or HiTrap S HP columns on an FPLC system (GE Healthcare, Piscataway, NJ). After being loaded, the proteins were eluted with a linear gradient of NaCl in 20 mM Tris (pH 7.4, 0−1 M NaCl). The peak fractions were pooled and dialyzed against 20 mM

Tris (pH 7.4) containing 50 mM NaCl. The ternary (syntaxin−SNAP-25−synaptobrevin) complex went through an initial purification step using a Q column (GE Healthcare) following the overnight assembly of the purified monomers. The minimal core complex was then further purified by size exclusion chromatography on a Superdex 200 HiLoad 16/60 prep grade column in standard buffer containing 300 mM NaCl as described previously (*29*).

Spin Labeling syt1C2AB. Single-cysteine mutants of syt1C2AB were spin-labeled as described previously using the sulfhydryl reactive spin-label MTSL, (1-oxyl-2,2,5,5-tetramethylpyrroline-3-methyl) methanethiosulfonate (Toronto Research Chemicals, North York, ON), at a 1:10 protein:MTSL molar ratio. Excess free spin-label was removed by passing the sample through a HiPrep 26/10 desalting column (GE Healthcare), and the spin-labeled protein was concentrated to 20−150 μM using either Centriprep or Centricon micro concentrators (Millipore, Billerica, MA).

Large Unilamellar Vesicles. 1-Palmitoyl-2-oleoyl-*sn*-glycero-3-phosphocholine (POPC) and 1-palmitoyl-2-oleoyl-*sn*-glycero-3-phosphoserine (POPS) (Avanti Polar Lipids, Alabaster, AL) were used to prepare large unilamellar vesicles (LUVs) with a POPC:POPS ratio of 3:1 as described previously (*28*). Liposomes containing the Ni(II) lipid chelate 1,2-dioleoyl-*sn*-glycero-3-{[*N*-(5-amino-1-carboxypentyl)iminodiacetic acid]succinyl} (nickel salt) [DOGS-NTA-Ni(II)] (Avanti Polar Lipids) were prepared in an identical manner with a POPC:POPS:DOGS-NTA-Ni(II) ratio of 65:25:10.

EPR Spectroscopy. EPR spectra were recorded on a Varian E-line 102 series X-band spectrometer fitted with a loop-gap resonator (Medical Advances, Milwaukee, WI). Spin-labeled samples of syt1C2AB contained protein concentrations that varied from 20 to 150 μM in the presence (1 mM Ca^{2+}) or absence of calcium (5 mM EDTA). The spectra from membrane-bound syt1C2AB were obtained in the presence of LUVs (50 mM total lipids) to ensure complete membrane binding and low surface densities of the protein. Unless otherwise noted, spectra with field sweeps of 100 G were recorded using 2 mW of incident microwave power and a 100 kHz modulation with an amplitude of 1 G.

The scaled mobility, M_s, of the EPR spectrum provides a relative measure of nitroxide mobility, where a value of 1 represents the most mobile and a value of 0 represents the least mobile EPR spectra that are obtained from the R1 side chain (Figure 1) in proteins. M_s is determined from the central line width of the EPR spectrum as given by eq 1.

$$M_s = \frac{\delta_{exp}^{-1} - \delta_i^{-1}}{\delta_m^{-1} - \delta_i^{-1}} \quad (1)$$

where δ_{exp} is the measured central line of the EPR spectrum and δ_i and δ_m are the corresponding values at the most immobilized and mobile sites observed in proteins, respectively. In this study, we used values of 2.1 G for δ_m and 8.4 G for δ_i (*30*).

To determine the position of the linker region and other sites when syt1C2AB is bound to membranes, continuous-wave power saturation experiments were performed in the presence and absence of a secondary paramagnetic species as described previously (*31, 32*). Collision parameters, Π, for each paramagnetic reagent were also determined by normalizing the values of $\Delta P_{1/2}$ by the central line width and the $P_{1/2}$ value for a solid sample of α,α'-diphenyl-β-picrylhydrazyl (DPPH) as described previously (*33*). Two empirical depth parameters were used to estimate the position of the linker in syt1C2AB relative to the membrane interface. The first Φ_1 given in eq 2 is based upon the ratio of oxygen and Ni(II)EDDA collision parameters.

$$\Phi_1 = \ln\left[\frac{\Pi^{oxy}}{\Pi^{Ni(II)EDDA}}\right] \quad (2)$$

The depth parameter Φ_1 was previously calibrated in membranes composed of POPC and POPS (*28, 34*). A second depth parameter, eq 3, which is expected to be more sensitive to the distance variation in the aqueous phase near the membrane interface is based upon the ratio of the DOGS-NTA-Ni(II) to Ni(II)EDDA collision parameters, $\Pi^{DOGS\text{-}Ni}$ and Π^{NiEDDA}, respectively.

$$\Phi_2 = \ln\left[\frac{\Pi^{DOGS\text{-}Ni}}{\Pi^{Ni(II)EDDA}}\right] \quad (3)$$

In this case, the ratio of the collision parameter for DOGS-NTA-Ni(II) versus Ni(II)EDDA is taken to eliminate the effects of steric differences at the labeled sites. The dependence of the depth parameter Φ_2 as a function of position is not known, and the first C2 domain of synaptotagmin 1, syt1C2A, was used to calibrate the parameter, since its orientation and position on POPC/POPS membranes are known. To make these measurements, R1-labeled mutants of the first C2 domain of synaptotagmin were produced as described previously (*28*) with labels that lie on the aqueous side of the membrane interface at positions 170, 176, 189, 193, 202, 217, 239, 240, and 256. The depth parameters, Φ_2, were then compared with the distances from the nitrogen on the nitroxide to the plane of the lipid phosphates using the previously determined orientation and depth of C2A (*28*). To orient the nitroxides at individual sites, the most likely rotamers for the first three dihedral angles of the R1 side chain were selected on the basis of previous crystallography results (*35*−*37*). Rotamers were eliminated which produced steric interference with other side chains or produced inconsistent positions of R1 with the values of the depth parameter Φ_1 obtained for each site. The allowed rotations of the last two dihedral angles were used to estimate the error in the position of the side chain.

Determining the Binding Affinity of the SNARE Complex for syt1C2AB. The binding of syt1C2AB to the SNARE complex was analyzed using EPR spectroscopy. The rate of exchange of syt1C2AB on and off the SNARE complex is slow relative to the EPR time scale. As a result, the EPR spectrum from a labeled site in syt1C2AB in the presence of the SNARE complex is a simple linear combination of the spectrum for unbound and bound syt1C2AB. In this case, the fraction of bound syt1C2AB, f_b, can be given by

$$f_b = \frac{A_f - A(0)}{A_f - A_b} \quad (4)$$

where $A(0)$ is the amplitude of the peak-to-peak central nitroxide resonance and A_f and A_b represent the intrinsic amplitudes of the central resonance obtained for free and SNARE-associated syt1C2AB, respectively.

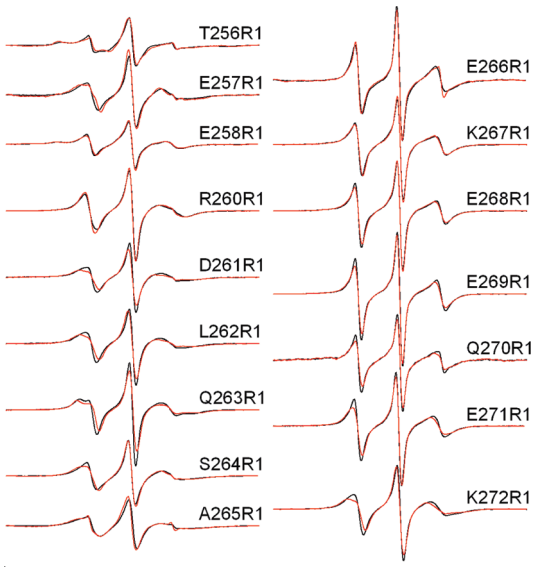

FIGURE 2: X-Band EPR spectra of single R1 substitutions in C2AB in the presence of Ca^{2+}. Aqueous spectra are colored black, and spectra of C2AB completely bound to POPC/POPS (75:25) vesicles are colored red. Spin-labeled mutants within the linker encompass residues 264−272, and mutants 256−263 cover the last β-strand in C2A. The spectra are normalized relative to each other, and the relative amplitudes provide an indication of relative nitroxide motion. The spectra are 100 G scans. The spin-labeled protein concentration in these experiments was 50 μM, with lipid concentrations ~1000-fold higher (≥50 mM). This lipid concentration is well in excess of that needed to completely bind syt1C2AB as shown previously (*11*).

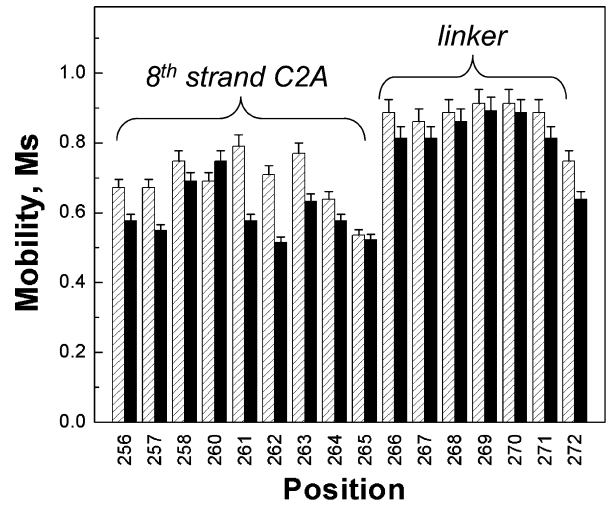

FIGURE 3: Scaled mobilities, M_s, for the spin-labeled sites within syt1C2AB that are located in the linker region or in the eighth β-strand of C2A. Values of M_s were calculated from the central line width of the EPR spectrum using eq 1. Aqueous values are shown with gray bars, and values for syt1C2AB bound to POPC/POPS (75:25) vesicles are shown with black bars. When proteins bound to lipid bilayers, there is a small decrease in the scaled mobility at some sites. Some of this decrease is likely due to a decrease in the level of protein rotation and attachment of C2A and C2B upon membrane binding. Several sites show larger changes upon binding, which may indicate changes in local structure or dynamics upon membrane association (see the text).

RESULTS

The Protein Segment Connecting C2A and C2B Is Unstructured in Solution and Bound to Bilayers. Sixteen singly labeled cysteine mutants were produced, expressed, and labeled as described in Materials and Methods. As indicated above, this fragment of synaptotagmin 1 is folded and is found to bind to membranes containing POPC and POPS (3:1) in a Ca^{2+}-dependent manner. Figure 2 shows the first-derivative X-band EPR spectra obtained from these R1 mutants in solution in the presence of Ca^{2+} and bound to lipid vesicles composed of POPC and POPS (3:1). Residues 256−265 are positioned in the last β-strand of C2A and lie at the edge of the β-sandwich. Residues 266−271 are thought to encompass the segment that connects C2A with C2B.

The spectra in Figure 2 arise from labels that exhibit a range of motion, with the broadest line shapes arising from sites in strand 8 of C2A, for example, sites 256, 258, 262, and 265. These EPR line shapes are similar to those that have been reported at other β-edge strand sites in cellular retinol binding protein (*38*). The most mobile line shapes arise from residues in the linker region, 266−271. These spectra correspond to nitroxides that have effective correlation times of approximately 1.5 ns with highly isotropic motion. Relatively minor changes in the spectrum are detected upon membrane binding. In the absence of Ca^{2+}, the EPR spectra obtained for the labeled sites shown in Figure 2 are unchanged from the Ca^{2+}-bound case (Supporting Information).

Shown in Figure 3 are the scaled mobilities calculated according to eq 4 for the 16 residues in syt1C2AB, both in solution and bound to membranes. The scaled mobility, M_s, provides a relative measure of nitroxide motion, where an M_s value of 1 represents the most mobile and a value of 0 represents the least mobile R1 side chains seen in proteins (*30*). This parameter is extracted from the peak-to-peak line width of the EPR spectrum, and it is largely determined by the label correlation time (*39*). For residues in the linker region, the scaled mobilities are high, typically 0.8−0.9, indicating that they represent some of the most mobile R1 EPR line shapes that are seen in proteins. Outside this region, the values of M_s are lower and range from ~0.5 to 0.8.

When bound to the lipid bilayer (Figure 3, black bars), many labeled sites show a small decrease in label mobility. The most significant changes take place at sites 261−263 near the point of attachment of the linker region to C2A. The addition of solutes such as Ficoll, which increases solution viscosity and slows the protein correlation time (*40*), produces little change in the EPR spectra from those of syt1C2AB. This indicates that the changes seen at sites 261−263 may be due to small structural changes or changes in dynamics at this β-strand edge upon membrane binding.

Parameters that are obtained from the EPR spectrum of R1, such as the central line width and second moment, are an indicator of the local structure at the labeled site. A plot of the reciprocal central line width (ΔH_0^{-1}) versus the reciprocal of the second moment ($\langle H^2 \rangle^{-1}$) yields a map that defines regions of different label contact and environment (*41, 42*). These data for the syt1C2AB spectra obtained in solution are shown in Figure 4. As indicated in this plot, residues encompassing the linker region have line shapes that are characteristic of unstructured protein segments or positions in loop segments.

The spectra shown in the presence of bilayers in Figure 2 were obtained under conditions where syt1C2AB was completely membrane-bound, so that the first and third Ca^{2+}-binding loops were contacting and penetrating the bilayer

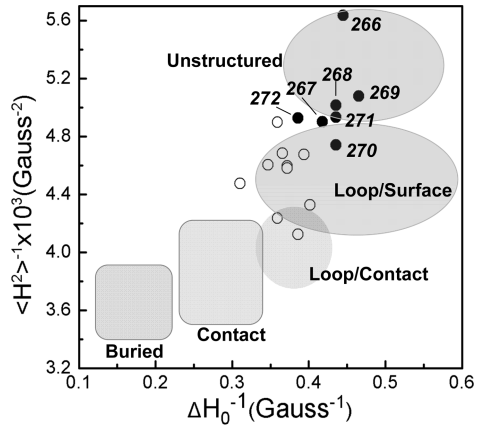

FIGURE 4: Plot of the reciprocal of the central line width (ΔH_0^{-1}) vs the reciprocal of the second moment ($\langle H^2 \rangle^{-1}$) of the EPR spectrum for the labeled sites in syt1C2AB. Residues that make up the flexible portion of the linker, 266−272, are denoted with solid circles. The empty circles represent sites outside the linker and in the eighth β-strand of C2A. Many sites within the linker have spectral characteristics of an unstructured protein segment; other sites in the linker resemble those in very dynamic loop segments. The shaded areas correspond to those defined previously, based upon EPR line shapes from R1 at sites in proteins of known structure (*42*).

Table 1: Depth Parameters, Φ_1, for syt1C2A and syt1C2AB[a]

mutant	Π^{oxy}	Π^{NiEDDA}	Φ_1
C2AB L262R1	0.13 ± 0.01	1.40 ± 0.1	−2.4 ± 0.1
C2AB Q263R1	0.14 ± 0.02	1.20 ± 0.1	−2.2 ± 0.1
C2AB S264R1	0.14 ± 0.02	0.99 ± 0.07	−2.2 ± 0.1
C2AB A265R1	0.13 ± 0.02	1.18 ± 0.08	−2.2 ± 0.1
C2AB Q266R1	0.17 ± 0.03	1.17 ± 0.10	−2.2 ± 0.1
C2AB K267R1	0.16 ± 0.02	2.0 ± 0.1	−2.5 ± 0.1
C2AB E268R1	0.22 ± 0.02	2.1 ± 0.1	−2.3 ± 0.1
C2AB E269R1	0.22 ± 0.03	2.2 ± 0.2	−2.3 ± 0.1

[a] Depth parameters for the singly R1-labeled sites when syt1C2A or syt1C2AB is completely bound to vesicles composed of POPC and POPS (75:25). Errors are based upon fits of the data to $P_{1/2}$.

interface (*11*). These data indicate that the linker between the two C2 domains remains flexible when the protein is membrane-bound. The data suggest that the two domains are interacting independently when associated with the membrane interface. There is no evidence of a Ca^{2+}-dependent change in the structure or dynamics of the linker region, and labels in the linker region do not show any evidence of tertiary contact. Such contact would have been expected at positions 267 and 271 if syt1C2AB assumed the conformation seen in the crystal structure (*18*).

Spin-Labels in the Linker Have an Aqueous Exposure and Lie 7−10 Å from the Plane of the Phosphates When syt1C2AB Is Membrane-Bound. To determine whether the linker region comes close to or penetrates the bilayer surface, power saturation experiments were performed to measure the exposure of R1 sites on the linker to the secondary paramagnetic species oxygen, and Ni(II)EDDA (see Materials and Methods). Shown in Table 1 are the collision parameters, Π^{oxy} and Π^{NiEDDA}, and the depth parameters, Φ_1, for residues 262−269 covering one edge of the β-strand on C2A though the linker region. The values of Φ_1 are all less than −2.0, which indicates that the labeled sites have an aqueous exposure and are more than 5 Å from the level of the lipid phosphates (*28*).

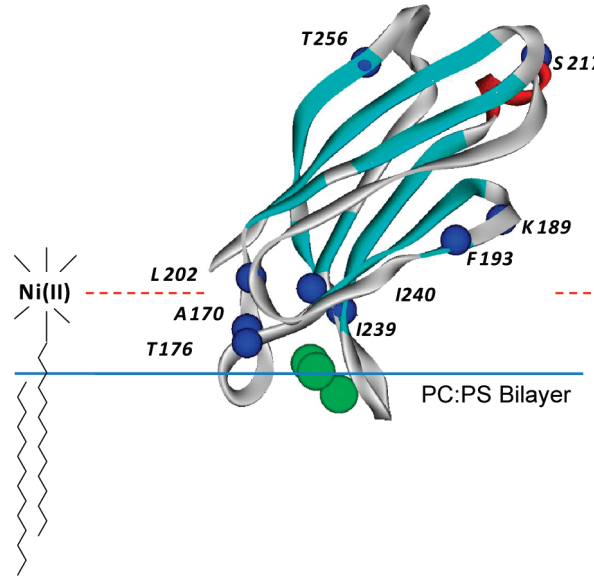

FIGURE 5: High-resolution model for syt1C2A (PDB entry 1BYN) (*15*). The domain is shown bound to bilayers composed of POPC and POPS with a depth of penetration and orientation that were previously determined via SDSL (*28*). This structure was used to calibrate the position parameter Φ_2 as described in Materials and Methods. This parameter is expected to be sensitive to the position of the label on the aqueous side of the bilayer interface and utilizes the lipid-bound nickel chelate, DOGS-NTA-Ni(II). Single-cysteine mutants were generated at the indicated residues (Cα atoms highlighted in blue) to incorporate a series of R1 labels (see Figure 1A) at varied positions off the bilayer interface.

To obtain a better estimate for the distance of the linker from the interface, we utilized a membrane-bound paramagnetic reagent, DOGS-NTA-Ni(II). In this Ni(II) lipid chelate, the metal center is believed to be extended into the aqueous phase so that the maximum concentration of the reagent resides in a layer that is approximately 14 Å above the membrane−lipid interface (*43*). Our expectation is that the rate of collision with DOGS-NTA-Ni(II) will drop off on either side of this layer but may be quite broad due to dynamic motion of lipids in the bilayer interface. To account for steric differences between labeled sites and to obtain a depth parameter, the collision frequency with DOGS-NTA-Ni(II) was referenced against Ni(II) EDDA, which is expected to diminish in concentration only near the interface (see Materials and Methods).

To calibrate this approach, we used the C2A domain from syt1. The orientation of this domain was previously determined on membranes composed of POPC and POPS (see Figure 5) (*28*), and the positions of labels placed within this domain are known relative to the membrane interface. The R1 spin-label was attached to the sites indicated in Figure 5, and measurements of Π^{oxy}, Π^{NiEDDA}, and Π^{DOGSNi} were taken for eight R1 mutants of C2A bound to extruded vesicle bilayers composed of POPC and POPS or POPC, POPS, and DOGS-NTA-Ni(II) (see Materials and Methods). The data obtained in these measurements are shown in Table 2, and the dependence of the depth parameter, Φ_2, upon the expected position of the R1 label relative to the membrane interface is shown in Figure 6.

Spin-labels on C2A at positions 176, 202, and 239 are located approximately 8−10 Å above the membrane surface, and they have the highest collision parameters, Π^{DOGSNi}, and the least negative depth parameters, Φ_2. The remaining sites

Table 2: Depth Parameters, Φ_2, for syt1C2A and syt1C2AB[a]

mutant	Π^{oxy}	Π^{NiEDDA}	$\Pi^{DOGS\text{-}NTA}$	Φ_2
C2A A170R1	0.27 ± 0.03	3.0 ± 0.2	0.18 ± 0.02	−2.8 ± 0.1
C2A T176R1	0.24 ± 0.02	2.6 ± 0.2	0.68 ± 0.04	−1.4 ± 0.1
C2A K189R1	0.26 ± 0.02	3.3 ± 0.2	0.07 ± 0.02	−3.9 ± 0.3
C2A F193R1	0.17 ± 0.02	1.4 ± 0.1	0.11 ± 0.02	−2.6 ± 0.2
C2A L202R1	0.30 ± 0.02	4.9 ± 0.3	0.41 ± 0.03	−2.5 ± 0.1
C2A I239R1	0.14 ± 0.01	1.2 ± 0.1	0.89 ± 0.05	−0.3 ± 0.1
C2A I240R1	0.12 ± 0.01	1.6 ± 0.1	0.06 ± 0.01	−3.3 ± 0.2
C2A S217R1	0.40 ± 0.04	3.7 ± 0.2	−	−
C2A T256R1	0.26 ± 0.02	3.4 ± 0.2	0.004 ± 0.01	−6.7 ± 2.2
C2AB L262R1	0.13 ± 0.01	1.4 ± 0.1	0.1 ± 0.01	−2.7 ± 0.1
C2AB Q263R1	0.14 ± 0.02	1.2 ± 0.1	0.1 ± 0.01	−2.6 ± 0.1
C2AB K267R1	0.16 ± 0.02	2.0 ± 0.1	1.10 ± 0.07	−0.6 ± 0.1
C2AB E268R1	0.22 ± 0.02	2.1 ± 0.1	0.57 ± 0.05	−1.3 ± 0.1
C2AB E269R1	0.22 ± 0.03	2.2 ± 0.2	1.39 ± 0.10	−0.5 ± 0.1

[a] Depth parameters for the singly R1-labeled sites when syt1C2A or syt1C2AB is completely bound to vesicles composed of POPC and POPS or POPC, POPS, and DOGS-NTA-Ni(II). Errors are based upon fits of the data to $P_{1/2}$.

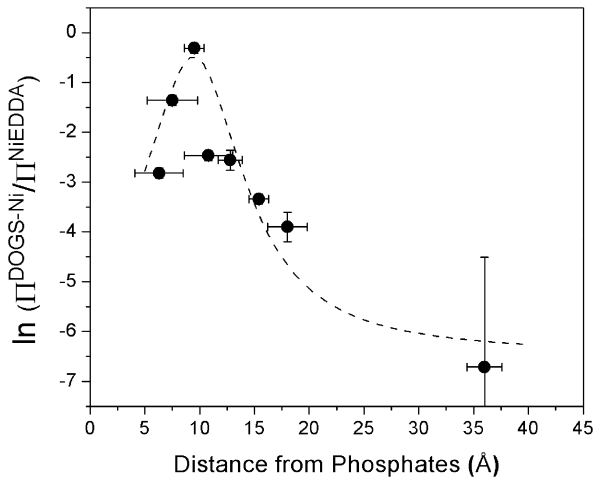

FIGURE 6: Correlation of the position or depth parameter Φ_2 at sites on syt1C2A as a function of distance from the membrane surface. The parameter Φ_2 was determined using $\Delta P_{1/2}$ values for Ni(II)-EDDA and DOGS-NTA-Ni(II) as given in eq 3. The distances of the R1 label on C2A were extracted from a model for membrane-bound syt1C2A (*28*) using the procedure described in Materials and Methods. The dashed line shows a Lorentzian centered around 9.5 Å.

are above or below 8−10 Å, and they have lower values of Π^{DOGSNi} and lower values of Φ_2. As seen in Figure 6, the value of Φ_2 appears to undergo a maximum as expected, and the position of this maximum lies at approximately 8−10 Å in these bilayers composed of POPC, POPS, and DOGS-NTA-Ni(II). In addition to the change in saturation behavior, the high rate of collision between R1 and Ni(II) leads to a slight broadening in the EPR spectra. This effect is most notable for the spectra obtained from sites 176, 202, and 239 (see the Supporting Information).

Depth measurements using DOGS-NTA-Ni(II) were made for several sites in the central linker for membrane-bound syt1C2AB. As shown in Table 2, the values of Π^{DOGSNi} are very high for labels in the linker (residues 267−269), and the values of Φ_2 for linker residues 267−269 in C2AB lie between the values obtained for sites 176 and 239 on C2A. These data indicate that the central linker is located at approximately the same distance as these residues in C2A, which is 7−10 Å above the membrane surface and near the region where the concentration of Ni(II) is a maximum for the DOGS-NTA-Ni(II)-containing liposomes. The EPR line shapes from the linker sites also indicate the linker is close to this Ni(II) layer, and the spectra from these sites show significant broadening due to collisional exchange with Ni(II) (see the Supporting Information).

The Linker between C2A and C2B Remains Flexible When syt1C2AB Binds to the Core SNARE Complex. To determine whether the linker in syt1 remains flexible when syt1C2AB binds to SNAREs or is directly involved in mediating interactions with SNAREs, EPR spectra were obtained from spin-labeled sites within the linker under conditions where syt1C2AB is bound to the core SNARE complex. The binding affinity of syt1C2AB was estimated by placing a spin-label at position 325 in the C2B domain of syt1C2AB, which resides within the polybasic region of C2B. This region is thought to make up a region of C2B that interacts with the SNARE complex (*12*). The spectra shown in Figure 7 for 325R1 were recorded in the absence and presence of the SNARE complex. This EPR spectrum broadens dramatically in the presence of the SNAREs, indicating that label at this site undergoes a decrease in the level of motion upon SNARE binding. The appearance of the broad hyperfine extrema in this spectrum of 325R1 (arrows Figure 7B) indicates that the change in the EPR spectrum results from tertiary contact at the labeled site. Similar changes are seen in other resides within the polybasic region of the C2B domain (data not shown) and are due to tertiary contact of the SNARE proteins at this site. Using this labeled site, the spectrum of 325R1 was recorded as a function of the concentration of the core SNARE complex, and the fraction of syt1C2A bound to the SNAREs, which was calculated according to eq 4, is presented in Figure 7A. The fit to these data yields an affinity of the soluble SNAREs for syt1C2AB of approximately 25 μM.

Shown in Figure 7B are EPR spectra recorded for site 256 in the eighth β-sheet of the C2A domain and four sites in the linker in the absence and presence of 120 μM SNARE complex. This concentration is sufficient for binding virtually all syt1C2AB according to the data obtained in Figure 7A. These spectra show essentially no change as a function of SNARE addition and indicate that the dynamics of the linker on the nanosecond time scale are not altered by the binding of syt1C2AB with the SNAREs. Furthermore, the lack of change in these spectra indicates that tertiary contact between these labeled sites in the linker, or nearby side chains in the linker, with the SNAREs is not taking place upon SNARE binding. Thus, sites within the linker connecting C2A and C2B do not directly contact the SNAREs.

DISCUSSION

Site-directed spin labeling is a powerful approach to obtaining information regarding backbone dynamics and tertiary contact at the labeled site. In this work, we used SDSL to examine the protein segment that links the first and second C2 domains in syt1. The data indicate that the region connecting the two C2 domains is highly dynamic and unstructured, and there is no evidence of tertiary interactions of spin-labeled side chains in this linker with other regions of the protein. The flexibility of the linker is maintained either in solution (with or without Ca^{2+}) or when the two C2 domains of syt1 are bound to POPC/POPS bilayers. Fur-

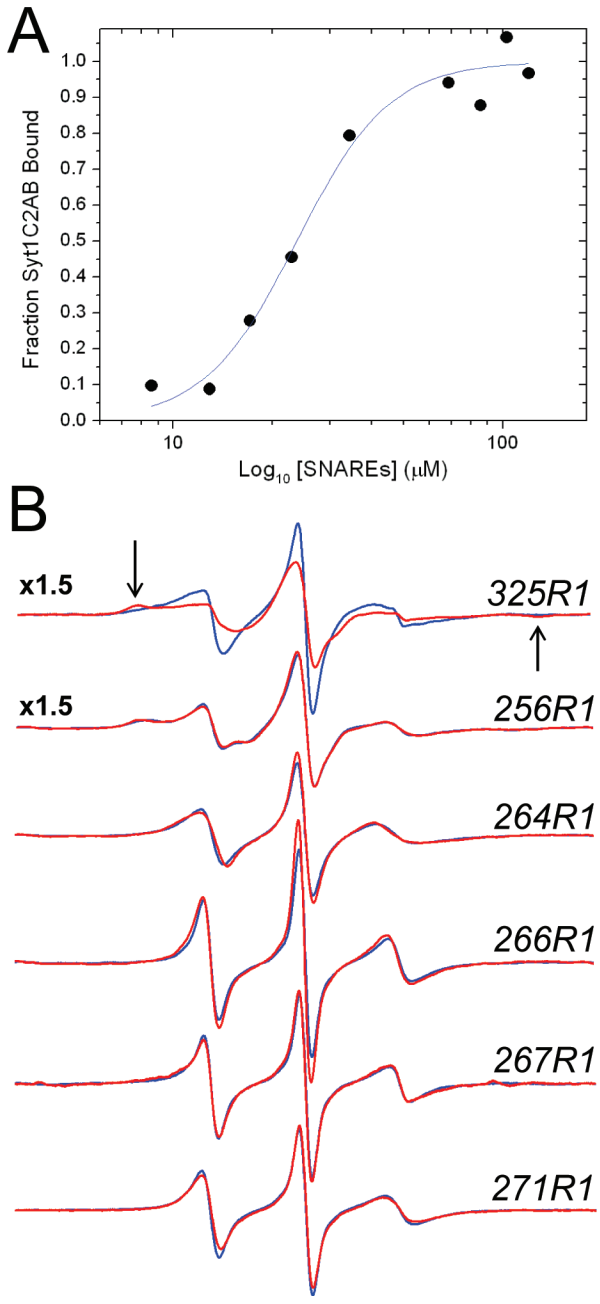

FIGURE 7: (A) Titration of the fraction of syt1C2AB bound to SNAREs as a function of the concentration of added soluble SNARE complex. The fraction of bound label was determined using eq 4. The fit to the data was made using a standard Hill equation and yielded an affinity of 24 μM. A slight apparent cooperativity is found in this binding when $n = 2$. In this titration, the concentration of syt1C2AB was held constant at 23 μM with a Ca^{2+} concentration of 1 mM. (B) EPR spectra of single R1 substitutions in the absence (blue trace) or presence (red trace) of 120 μM SNARE complex in the presence of 1 mM Ca^{2+}. Site 325 is located in the C2B domain and is likely at a site that is involved in tertiary contact with the SNAREs. The arrows indicate the position of the hyperfine extrema in this spectrum. Site 256 lies within the eighth β-strand in the C2A domain, and sites 264, 266, 267, and 271 lie within the linker connecting C2A and C2B. The amplitudes of these EPR spectra are normalized against the second integral of the EPR spectrum and are expanded by a factor of 1.5 for 325R1 and 256R1.

thermore, the linker remains dynamic and unstructured when syt1C2AB is bound to the core SNARE complex, and the sites examined within the linker do not directly interact with the SNARE complex.

These data also suggest that the two C2 domains in syt1 do not directly interact. A direct interaction of the two C2 domains, as indicated in the crystal structure (*18*), should restrain the linker and bring certain side chains within the linker into tertiary contact with other regions of syt1. However, these interactions are not seen, and there is no evidence of a significant change in local ordering within the linker with addition of Ca^{2+}. These results are consistent with NMR data showing that C2A and C2B have the same chemical shifts and do not interact in solution (*9*). However, the data obtained here also suggest that the two C2 domains function independently when syt1C2AB is bound to membranes or to SNAREs, since the dynamics of the linker are unchanged upon membrane or SNARE association.

The interactions of syt1 with the SNAREs have been reported to be mediated by the two C2 domains of syt1 (for example, refs *12*, *13*, and *44*), and models in which the linker between C2A and C2B straddles the bilayer have been proposed (*4, 45*). The measurements made here indicate that the flexibility of the linker is maintained when syt1C2AB is bound to the SNAREs. This result is consistent with a report indicating that syt1−SNARE interactions are largely mediated by C2B (*12, 46*) and that there may be multiple binding modes for the syt1−SNARE interaction (*12*). Previous data obtained from single-molecule FRET indicated that sites within the linker were in the proximity of the SNARE complex when syt1 was bound (*13*). The results obtained here indicate that while residues within the linker might be close to the SNAREs when syt1 is bound, they do not directly interact with the SNAREs. However, the measurements made here are not entirely analogous to these FRET measurements, since they have not yet been carried out in the presence of membrane-bound SNAREs.

At present, the mechanism by which syt1 triggers neuronal exocytosis is not known. Synaptotagmin 1 appears to interact both with SNAREs and with membranes (*45, 47*), and it is likely that both these interactions are necessary for the action of syt1 (*12, 48*). Many models for syt1-regulated membrane fusion are consistent with the results found here and require that the two C2 domains interact independently. For example, it has been proposed that C2A and C2B bind to the vesicle and target (plasma) membrane, respectively, thereby assuming a trans configuration. This requires that the protein segment connecting the two domains be flexible (*10*). C2A and C2B are also reported to have different lipid specificities, where C2B appears to have a higher affinity for $PI(4,5)P_2$, which is found in the plasma membrane (*49*). On the basis of this finding, it has been suggested that the two C2 domains of syt1 may target different membranes under different conditions, again requiring that the linker be flexible. However, the length of the linker appears to be important. Previous work demonstrated that lengthening the linker abolishes the interaction between syt1C2AB and the SNAREs and decreases the membrane fusion efficiency (*50*). The results imply that while the two domains may be flexibly linked, the relative position or separation between the two domains is important.

The data shown in Figure 7 indicate that the affinity of the core SNARE complex for syt1C2AB in solution is approximately 25 μM. This is 3 orders of magnitude weaker than the apparent affinity measured for syt1C2AB toward the membrane-bound SNARE complex (*51*). This dramatic

discrepancy and the increased affinity of syt1C2AB toward membrane-bound SNAREs are expected if there are multiple binding sites for syt1, for example, if syt1C2AB makes simultaneous interactions with both the membrane interface and the SNAREs. Indeed, previous work suggests that there is a complex formed among syt1, SNAREs, and the membrane interface (*12*). In this case, the free energies of interaction of syt1C2AB toward SNAREs and the lipid bilayer should be roughly additive.

Previous work using site-directed spin labeling indicated that both the first and third Ca^{2+}-binding loops of the C2A and C2B domains of syt1 penetrated the bilayer when syt1C2AB was membrane-bound (*11*). This model was based upon depth data from SDSL, and the high-resolution solution structures of the individual C2A and C2B domains. In this model, the extensions of the C-terminal end of C2A and the N-terminal end of C2B are projected toward the bilayer interface, but no data on the separation between domains or the position of the linker were obtained. The collision accessibility data obtained here using Ni(II)EDDA or DOGS-NTA-Ni(II) indicate that the linker does not penetrate the bilayer but resides on the aqueous side of the membrane−solution interface. At present, we are using data on the linker, depth constraints, and distance constraints obtained from double electron−electron resonance to generate a more refined structural model for membrane-associated syt1C2AB.

Information about the position of protein segments lying on the aqueous side of the membrane solution interface can be obtained using gradients of charged paramagnetic regents, such as chromium oxalate (*52, 53*). In this approach, high surface charge densities and low ionic strengths are typically utilized to establish a concentration gradient of the charged reagent. The lipid chelate DOGS-NTA-Ni(II) was used previously to identify spin-labeled sites on KcsA that lie near the membrane interface (*43*). This work demonstrates that this lipid−Ni(II) chelate can also be used to localize spin-labels on proteins at positions off the membrane interface and that the Ni(II) bound to DOGS-NTA has a maximum concentration in a region that lies 8−10 Å from the layer of the phosphates on the membrane interface. The collision parameters for DOGS-NTA-Ni(II) will be sensitive to the relative diffusion rates of DOGS-NTA-Ni(II) within different bilayers or different membrane regions. This may require different calibrations on different membrane surfaces and might lead to interesting effects in membrane proteins if there are regions of immobilized lipid near labeled sites.

In summary, the position and conformation of the region that links C2A and C2B in syt1 were determined by site-directed spin labeling. This region of syt1C2AB is flexible and largely unstructured in solution, with or without Ca^{2+}, and when bound to the membrane interface. When syt1C2AB is bound to membranes, residues within the linker reside approximately 7−10 Å on the aqueous side of the lipid phosphates. The linker remains flexible and unstructured when syt1C2AB is bound to the SNARE complex, and it does not directly participate in syt1−SNARE interactions. These results are consistent with models for membrane fusion in which the two C2 domains interact independently, on membrane or protein sites.

ACKNOWLEDGMENT

We thank Drs. Reinhard Jahn and Dirk Fasshauer (Max-Planck-Institute for Biophysical Chemistry) for providing DNA for the His-tagged SNARE proteins, Drs. Wayne Hubbell and Christian Altenbach (University of California, Los Angeles) for LabView software used in the EPR data analysis, and members of Dr. Lukas Tamm's laboratory for assistance with the assembly of the SNARE complexes.

SUPPORTING INFORMATION AVAILABLE

Additional EPR spectra obtained for syt1C2AB in solution in the presence and absence of Ca^{2+}, EPR spectra for syt1C2A, and EPR spectra for bound syt1C2AB in the presence of DOGS-NTA-Ni(II). This material is available free of charge via the Internet at http://pubs.acs.org.

REFERENCES

1. Jahn, R., Lang, T., and Sudhof, T. C. (2003) Membrane Fusion. *Cell 112*, 519–533.
2. Rothman, J. E. (1994) Mechanisms of intracellular protein transport. *Nature 372*, 55–63.
3. Sudhof, T. C. (2004) The synaptic vesicle cycle. *Annu. Rev. Neurosci. 27*, 509–547.
4. Koh, T.-W., and Bellen, H. J. (2003) Synaptotagmin I, a Ca^{2+} sensor for neurotransmitter release. *Trends Neurosci. 26*, 413–422.
5. Rizo, J., Chen, X., and Arac, D. (2006) Unraveling the mechanisms of synaptotagmin and SNARE function in neurotransmitter release. *Trends Cell Biol. 16*, 339–350.
6. Chapman, E. R. (2008) How does synaptotagmin trigger neurotransmitter release? *Annu. Rev. Biochem. 77*, 615–641.
7. Bhalla, A., Chicka, M. C., Tucker, W. C., and Chapman, E. R. (2006) Ca^{2+}-synaptotagmin directly regulates t-SNARE function during reconstituted membrane fusion. *Nat. Struct. Mol. Biol. 13*, 323–330.
8. Martens, S., Kozlov, M. M., and McMahon, H. T. (2007) How synaptotagmin promotes membrane fusion. *Science 316*, 1205–1208.
9. Arac, D., Chen, X., Khant, H. A., Ubach, J., Ludtke, S. J., Kikkawa, M., Johnson, A. E., Chiu, W., Sudhof, T. C., and Rizo, J. (2006) Close membrane-membrane proximity induced by Ca^{2+}-dependent multivalent binding of synaptotagmin-1 to phospholipids. *Nat. Struct. Mol. Biol. 13*, 209–217.
10. Stein, A., Radhakrishnan, A., Riedel, D., Fasshauer, D., and Jahn, R. (2007) Synaptotagmin activates membrane fusion through a Ca^{2+}-dependent trans interaction with phospholipids. *Nat. Struct. Mol. Biol. 14*, 904–911.
11. Herrick, D. Z., Sterbling, S., Rasch, K. A., Hinderliter, A., and Cafiso, D. S. (2006) Position of synaptotagmin I at the membrane interface: Cooperative interactions of tandem C2 domains. *Biochemistry 45*, 9668–9674.
12. Dai, H., Shen, N., Arac, D., and Rizo, J. (2007) A quaternary SNARE-synaptotagmin-Ca^{2+}-phospholipid complex in neurotransmitter release. *J. Mol. Biol. 367*, 848–863.
13. Bowen, M. E., Weninger, K., Ernst, J., Chu, S., and Brunger, A. T. (2005) Single-molecule studies of synaptotagmin and complexin binding to the SNARE complex. *Biophys. J. 89*, 690–702.
14. Sutton, R. B., Davletov, B. A., Berghuis, A. M., Sudhof, T. C., and Sprang, S. R. (1995) Structure of the first C2 domain of synaptotagmin I: A novel Ca^{2+}/phospholipid-binding fold. *Cell 80*, 929.
15. Shao, X., Fernandez, I., Sudhof, T. C., and Rizo, J. (1998) Solution structures of the Ca^{2+}-free and Ca^{2+}-bound C2A domain of synaptotagmin I: Does Ca^{2+} induce a conformational change? *Biochemistry 37*, 16106–16115.
16. Fernandez, I., Arac, D., Ubach, J., Gerber, S. H., Shin, O., Gao, Y., Anderson, R. G., Sudhof, T. C., and Rizo, J. (2001) Three-dimensional structure of the synaptotagmin 1 C2B-domain: Synaptotagmin 1 as a phospholipid binding machine. *Neuron 32*, 1057–1069.
17. Cheng, Y., Sequeira, S. M., Malinina, L., Tereshko, V., Sollner, T. H., and Patel, D. J. (2004) Crystallographic identification of

Ca^{2+} and Sr^{2+} coordination sites in synaptotagmin I C2B domain. *Protein Sci. 13*, 2665–2672.
18. Fuson, K. L., Montes, M., Robert, J. J., and Sutton, R. B. (2007) Structure of human synaptotagmin 1 C2AB in the absence of Ca^{2+} reveals a novel domain association. *Biochemistry 46*, 13041–13048.
19. Garcia, R. A., Forde, C. E., and Godwin, H. A. (2000) Calcium triggers an intramolecular association of the C2 domains in synaptotagmin. *Proc. Natl. Acad. Sci. U.S.A. 97*, 5883–5888.
20. Hubbell, W. L., Gross, A., Langen, R., and Lietzow, M. A. (1998) Recent advances in site-directed spin labeling of proteins. *Curr. Opin. Struct. Biol. 8*, 649–656.
21. Hubbell, W. L., Cafiso, D. S., and Altenbach, C. (2000) Identifying conformational changes with site-directed spin labeling. *Nat. Struct. Biol. 7*, 735–739.
22. Columbus, L., and Hubbell, W. L. (2002) A new spin on protein dynamics. *Trends Biochem. Sci. 27*, 288–295.
23. Fanucci, G. E., and Cafiso, D. S. (2006) Recent advances and applications of site-directed spin labeling. *Curr. Opin. Struct. Biol. 16*, 644–653.
24. Klug, C. S., and Feix, J. B. (2008) Methods and applications of site-directed spin labeling EPR spectroscopy. *Methods Cell Biol. 84*, 617–658.
25. Sambrook, J., Fritsch, E. F., and Maniatis, T. (1989) *Molecular Cloning: A Laboratory Manual*, Cold Spring Harbor Laboratory Press, Plainview, NY.
26. Rufener, E., Frazier, A. A., Wieser, C. M., Hinderliter, A., and Cafiso, D. S. (2005) Membrane-bound orientation and position of the synaptotagmin C2B domain determined by site-directed spin labeling. *Biochemistry 44*, 18–28.
27. Buser, C. A., Sigal, C. T., Resh, M. D., and McLaughlin, S. (1994) Membrane binding of myristylated peptides corresponding to the NH2 terminus of Src. *Biochemistry 33*, 13093–13101.
28. Frazier, A. A., Roller, C. R., Havelka, J. J., Hinderliter, A., and Cafiso, D. S. (2003) Membrane-bound orientation and position of the synaptotagmin I C2A domain by site-directed spin labeling. *Biochemistry 42*, 96–105.
29. Fasshauer, D., Eliason, W. K., Brunger, A. T., and Jahn, R. (1998) Identification of a minimal core of the synaptic SNARE complex sufficient for reversible assembly and disassembly. *Biochemistry 37*, 10354–10362.
30. Langen, R., Cai, K., Altenbach, C., Khorana, H. G., and Hubbell, W. L. (1999) Structural features of the C-terminal domain of bovine rhodopsin: A site-directed spin-labeling study. *Biochemistry 38*, 7918–7924.
31. Altenbach, C., Greenhalgh, D. A., Khorana, H. G., and Hubbell, W. L. (1994) A collision gradient-method to determine the immersion depth of nitroxides in lipid bilayers. Application to spin-labeled mutants of bacteriorhodopsin. *Proc. Natl. Acad. Sci. U.S.A. 91*, 1667–1671.
32. Victor, K., and Cafiso, D. S. (1998) Structure and position of the N-terminal binding domain of pp60src at the membrane interface. *Biochemistry 37*, 3402–3410.
33. Farahbakhsh, Z. T., Altenbach, C., and Hubbell, W. L. (1992) Spin-labeled cysteines as sensors for protein-lipid interaction and conformation in rhodopsin. *Photochem. Photobiol. 56*, 1019–1033.
34. Frazier, A. A., Wisner, M. A., Malmberg, N. J., Victor, K. G., Fanucci, G. E., Nalefski, E. A., Falke, J. J., and Cafiso, D. S. (2002) Membrane orientation and position of the C2 domain from cPLA2 by site-directed spin labeling. *Biochemistry 41*, 6282–6292.
35. Langen, R., Oh, K. J., Cascio, D., and Hubbell, W. L. (2000) Crystal structures of spin labeled T4 lysozyme mutants: Implications for the interpretation of EPR spectra in terms of structure. *Biochemistry 39*, 8396–8405.
36. Guo, Z., Cascio, D., Hideg, K., Kalai, T., and Hubbell, W. L. (2007) Structural determinants of nitroxide motion in spin-labeled proteins: Tertiary contact and solvent-inaccessible sites in helix G of T4 lysozyme. *Protein Sci. 16*, 1069–1086.
37. Guo, Z., Cascio, D., Hideg, K., and Hubbell, W. L. (2008) Structural determinants of nitroxide motion in spin-labeled proteins: Solvent-exposed sites in helix B of T4 lysozyme. *Protein Sci. 17*, 228–239.
38. Lietzow, M. A., and Hubbell, W. L. (2004) Motion of spin label side chains in cellular retinol-binding protein: Correlation with structure and nearest-neighbor interactions in an antiparallel β-sheet. *Biochemistry 43*, 3137–3151.
39. Columbus, L., and Hubbell, W. L. (2004) Mapping backbone dynamics in solution with site-directed spin labeling: GCN4-58 bZip free and bound to DNA. *Biochemistry 43*, 7273–7287.
40. Columbus, L., Kalai, T., Jeko, J., Hideg, K., and Hubbell, W. L. (2001) Molecular motion of spin labeled side chains in α-helices: Analysis by variation of side chain structure. *Biochemistry 40*, 3828–3846.
41. McHaourab, H. S., Lietzow, M. A., Hideg, K., and Hubbell, W. L. (1996) Motion of spin-labeled side chains in T4 lysozyme. Correlation with protein structure and dynamics. *Biochemistry 35*, 7692–7704.
42. Isas, J. M., Langen, R., Haigler, H. T., and Hubbell, W. L. (2002) Structure and dynamics of a helical hairpin and loop region in annexin 12: A site-directed spin labeling study. *Biochemistry 41*, 1464–1473.
43. Gross, A., and Hubbell, W. L. (2002) Identification of protein side chains near the membrane-aqueous interface: A site-directed spin labeling study of KcsA. *Biochemistry 41*, 1123–1128.
44. Chapman, E. R., Hanson, P. I., An, S., and Jahn, R. (1995) Ca^{2+} regulates the interaction between synaptotagmin and syntaxin 1. *J. Biol. Chem. 270*, 23667–23671.
45. Bai, J., and Chapman, E. R. (2004) The C2 domains of synaptotagmin: Partners in exocytosis. *Trends Biochem. Sci. 29*, 143–151.
46. Rickman, C., Archer, D. A., Meunier, F. A., Craxton, M., Fukuda, M., Burgoyne, R. D., and Davletov, B. (2004) Synaptotagmin Interaction with the Syntaxin/SNAP-25 Dimer Is Mediated by an Evolutionarily Conserved Motif and Is Sensitive to Inositol Hexakisphosphate. *J. Biol. Chem. 279*, 12574–12579.
47. Brunger, A. T. (2005) Structure and function of SNARE and SNARE-interacting proteins. *Q. Rev. Biophys. 38*, 1–47.
48. Lynch, K. L., Gerona, R. R. L., Larsen, E. C., Marcia, R. F., Mitchell, J. C., and Martin, T. F. J. (2007) Synaptotagmin C2A loop 2 mediates Ca^{2+}-dependent SNARE interactions essential for Ca^{2+}-triggered vesicle exocytosis. *Mol. Biol. Cell 18*, 4957–4968.
49. Bai, J., Tucker, W. C., and Chapman, E. R. (2004) PIP2 increases the speed of response of synaptotagmin and steers its membrane-penetration activity toward the plasma membrane. *Nat. Struct. Mol. Biol. 11*, 36–44.
50. Bai, J., Wang, C.-T., Richards, D. A., Jackson, M. B., and Chapman, E. R. (2004) Fusion pore dynamics are regulated by synaptotagmin-t-SNARE interactions. *Neuron 41*, 929–942.
51. Tang, J., Maximov, A., Shin, O. H., Dai, H., Rizo, J., and Sudhof, T. C. (2006) A complexin/synaptotagmin 1 switch controls fast synaptic vesicle exocytosis. *Cell 126*, 1175–1187.
52. Lin, Y., Nielsen, R., Murray, D., Hubbell, W. L., Mailer, C., Robinson, B. H., and Gelb, M. H. (1998) Docking phospholipase A2 on membranes using electrostatic potential-modulated spin relaxation magnetic resonance. *Science 279*, 1925–1929.
53. Ball, A., Nielsen, R., Gelb, M. H., and Robinson, B. H. (1999) Interfacial membrane docking of cytosolic phospholipase A2 C2 domain using electrostatic potential-modulated spin relaxation magnetic resonance. *Proc. Natl. Acad. Sci. U.S.A. 96*, 6637–6642.

BI801470M